6th Workshop on Metallization and Interconnection for Crystalline Silicon Solar Cells, 2016

A comprehensive study of intermetallic compounds in solar cell interconnections and their growth kinetics

Torsten Geipel[a,*], Monja Moeller[b], Achim Kraft[a], Ulrich Eitner[a]

[a]*Fraunhofer Institute for Solar Energy Systems ISE, Heidenhofstrasse 2, 79110 Freiburg, Germany*
[b]*Christian-Albrechts-University Kiel, Christian-Albrechts-Platz 4, 24118 Kiel, Germany*

Abstract

Intermetallic compounds (IMC) in soldered interconnections influence the reliability of PV modules. Thus, the microstructure of solar cell interconnections and the growth of IMCs are to be investigated in this paper. Sn60Pb40 and Sn41Bi57Ag2 are chosen as alloy coatings of copper interconnectors and semi-automatically soldered to screen-printed front Ag-busbars of industrial mono-crystalline solar cells. The microstructure of the solder bonds is characterized with metallographic cross sections and confocal laser microscopy, as well as scanning electron microscopy and electron dispersive x-ray spectroscopy. The cross section samples are isothermally aged between 85 °C to 150 °C and for 15 hour to 155 hour to obtain the kinetic parameters of a diffusion-based growth model of the IMCs. The model is used to estimate the IMC thickness after 3000 h at 85 °C, and after 600 thermal cycles as well as after 25 years in the outdoor location Freiburg, Germany. It is found that extensive microstructural changes take place within the solder bonds during thermal aging. Grain coarsening within the solder matrix, in particular for Sn41Bi57Ag2 solders, is observed, which can lead to an entire Sn depletion of the solder matrix. Moreover, non-uniform Sn penetration and IMC growth at cavities and lead-glass particles of the busbar are observed for both solders, which is discussed in terms of its effect on metallization adhesion. Eventually, simulating the IMC growth for 3000 h at 85 °C forecasts a 3.7 μm thick Ag_3Sn IMC at the busbar for the Sn41Bi57Ag2 solder compared to 2.6 μm for Sn60Pb40. The prognosis of the IMC thickness after 25 years in Freiburg yields an Ag_3Sn thickness of 1.3 μm for Sn41Bi57Ag2.

Keywords: Photovoltaic module, Interconnection, Soldering, Intermetallic compounds, Intermetallic phase growth, Activation energy, Reliability

1. Introduction

Photovoltaic modules are designed to survive 25 to 30 years of outdoor operation, and improving their lifetime vastly decreases the levelized costs of electricity of photovoltaic systems [1]. Against this background, the quality of series interconnection of crystalline silicon solar cells into strings, which is part of the PV module integration

*Corresponding author. Tel.: +49-761-4588-5023 ; fax: +49-761-4588-9193

process, has a direct impact on the reliability of the PV module. Hence, understanding of solder bonds and their failure mechanisms can improve the reliability of PV modules.

The existence and growth of intermetallic compounds (IMC) within solder bonds influences the lifetime of the interconnections. After the joining process, IMCs exist within the solder matrix and, in most cases, at the interfaces to the solar cell metallization and the copper core of the ribbon as uniform and thin layers. They are an indication for a proper mechanical and electrical bond [2]. However, IMCs grow due to solid state aging at elevated temperatures or even storage at room temperature. Owing to their brittleness and the large mismatch of coefficients of thermal expansion (CTE) of the involved materials in the joint ($CTE_{Si} \approx 2.6 \times 10^{-6}\,K^{-1}$ and $CTE_{Cu} \approx 17 \times 10^{-6}\,K^{-1}$) cracks can easily be induced and propagated when the bond is exposed to thermal cycles or mechanical load [3, 4, 5, 6, 7].

In this paper we describe the microstructural changes of PV module solder bonds observed during thermal aging. Interconnector ribbons with a standard lead-based Sn60Pb40 solder coating along with a low melting point solder Sn41Bi57Ag2, which is under consideration for the interconnection of temperature sensitive high-efficiency solar cells, is used in the experimental investigation [8].

The growth kinetics of IMCs in PV module solder bonds is modeled. The model's Arrhenius parameters are obtained by systematic aging studies at varying temperatures. The model is then used to simulate the IMC growth during accelerated aging tests and during outdoor operation of a PV module in the location Freiburg, Germany.

The work presented here extends and deepens previous investigations of IMCs in solar cell interconnections [9, 10, 11]. Particularly, a direct comparison of the bismuth-based solder coating to standard lead-based solder and modeling of the phase growth with non-isothermal temperature profiles are new aspects presented in this work.

Nomenclature

CTE	coefficient of thermal expansion
$D(T)$	Diffusion coefficient
D_0	Pre-exponential factor
IMC	Intermetallic compound
k_B	Boltzmann constant
MAE	Mean absolute error
N_A	Avogadro constant
Q	Activation energy
R	Gas constant
T	Absolute temperature
t	Aging time
$\overline{x^2(t, T)}$	Mean square diffusion distance
$x(t, T)$	Intermetallic layer thickness
x_0	Initial intermetallic layer thickness

---

2. Materials and methods

2.1. Experimental

Since the eventual goal of this investigation is to describe and model the kinetics of the IMC growth within PV module solder bonds, the experimental part requires systematic isothermal aging of soldered interconnections at various temperatures, and measurement of the IMC layer thickness at defined time steps. Therefore, the front busbars of industrial, mono-crystalline solar cells are interconnected using Cu ribbons with the solder coatings Sn60Pb40 and Sn41Bi57Ag2. For the interconnection process a semi-automatic contact soldering station is used, that is depicted in Fig. 1a. The most important material properties and processing conditions are summarized in Table 1.

Then, the interconnected solar cells are cut, embedded, mechanically ground and polished to obtain metallographic cross sections [12]. The samples are divided into four groups which are isothermally aged at temperatures between

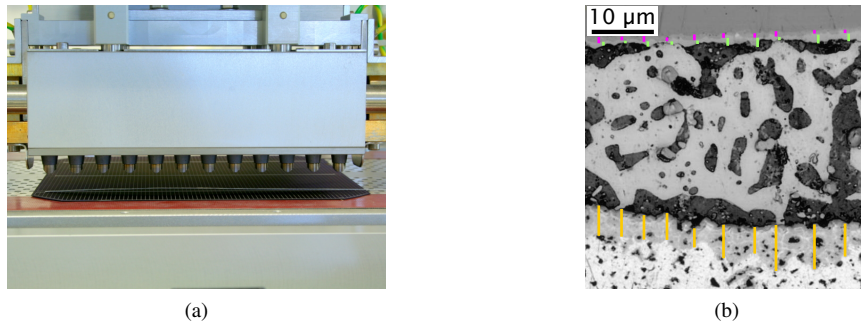(a)   (b)

Fig. 1. (a) Semi-automatic soldering station with solar cell and ribbon on heating chuck. (b) Confocal laser microscope image and measuring lines for IMC thickness determination.

Table 1. Solder coatings and processing conditions

Solder coating	Sn60Pb40	Sn41Bi57Ag2
Ribbon dimensions [mm^2]	0.2×1.5	0.18×1.5
Coating thickness [µm]	$15 - 25$	$15 - 25$
Melting temperature [°C]	183	139
Set heating chuck temperature [°C]	175	135
Set soldering temperature [°C]	250	200
Soldering time [s]	1.2	1.2
Down-holding time [s]	4	4

85 °C to 150 °C respectively depending on the melting temperature of the solder. The temperatures are chosen to allow the extraction of the activation energy of the IMC growth process and to obtain measurable IMCs on a short time scale[1]. Aging of the cross section samples allows the investigation of nearly the same position before and after the test. The cross section samples need to be polished prior to the metallographic inspection after thermal aging. The time steps, after which the solder bonds are characterized, are 15 h, 85 h and 155 h and for selected samples 500 h as well as 750 h.

The IMC thickness is measured with confocal laser microscopy. 30 parallel measurement lines are defined across the intermetallic layer and distributed over the whole cross section. The measurement process is illustrated in Fig. 1b, where a cross section of a solder bond with indicated measurement lines is shown.

2.2. Simulation

The growth of the intermetallic layers is governed by the time which the atoms need to diffuse through the already existing intermetallic layer and to rearrange the atomic structure [14]. A layer growth that is solely driven by diffusion is assumed in this work. The increasing extent of the intermetallic layer and, in turn, the increasing amount of time for atoms to diffuse through it leads to a slowdown of further growth, which gives the growth kinetics its typical parabolic shape over time.

Starting from a solution of Fick's second law and a random walk treatment, the mean square diffusion distance $\overline{x^2(t,T)}$ after time t and at the absolute temperature T is [15]:

$$\overline{x^2(t,T)} = 2D(T)t \tag{1}$$

---

[1]Therefore, the choice of aging temperatures is neither related to the PV module temperature under outdoor conditions, which, assuming proper operation, is limited to approximately 80 °C nor accelerated aging test according to IEC 61215 [13].

$D(T)$ is the diffusion coefficient and its temperature dependency is described by the Arrhenius relationship.

$$D(T) = D_0 \exp\left(-\frac{Q}{RT}\right) \tag{2}$$

with D_0 being the pre-exponential factor, Q the activation energy, and R the gas constant.

Providing an initial intermetallic layer thickness x_0 and combining equations 1 and 2, the intermetallic layer thickness $x(t, T)$ is expressed with equation 3.

$$x(t, T) = \sqrt{2D_0 \exp\left(-\frac{Q}{RT}\right)t} + x_0 \tag{3}$$

If the natural logarithm is taken on both sides of equation 3, a linear relationship between $1/T$ and $\ln[x(t, T) - x_0]$ exists, such that Q is obtained using the slope of equation 4.

$$\ln[x(t, T) - x_0] = \frac{\ln(2D_0 t)}{2} - \frac{Q}{2R}\frac{1}{T} \tag{4}$$

In order to determine the activation energy, thermal aging experiments need to be done at three or more different temperatures. For each time step with different temperatures a straight line in the form of equation 4 is derived. Since Q is assumed constant over the course of the growth reaction a weighted average is taken over all slopes. Furthermore, D_0 is calculated by non-linear fitting of the experimental layer thickness $x(t, T)$ to equation 3 with Q, T and x_0 as constant parameters. The calculation of $x(t, T)$ for non-constant temperature progressions, such as under thermal cycling conditions, requires a numerical algorithm that is implemented in Matlab.

3. Results

3.1. Microstructural changes and intermetallic phase growth

A Sn60Pb40 solder bond in the initial conditions after the soldering process is shown in Fig. 2a. The solder matrix is characterized by a uniform distribution of Sn-rich and Pb-rich grains. The diameter of those ranges from 0.5 μm to 10 μm, which is mainly dependent on the cooldown process, whereas a rapid cooldown leads to a finer grain structure. The grain structure then again influences the mechanical properties of the solder bond [16]. With that, Pb has certain technical advantages in solder compositions [7]. Among others, its inherent ductility absorbs (thermo-)mechanical stress more easily.

During the pre-tinning and the soldering process, the copper core and respectively the busbar metallization is partially dissolved into the molten solder. The high concentration of foreign atoms in the liquid solder at the interface leads to the formation of intermetallic compounds according to the phase diagrams of the respective alloy systems [2, 6, 17, 18]. At the interface from the Sn60Pb40 matrix to the Cu core of the ribbon a 0.3 μm Cu_6Sn_5 intermetallic phase is formed, that is characterized by a scallop-type morphology [19, 20]. Moreover, at the interface to the Ag busbar, an Ag_3Sn intermetallic layer of 0.7 μm thickness is formed during the soldering process [21]. It is usually uniform, but excessive soldering conditions can result in plate-like protrusions into the solder matrix [7].

As can be seen in Fig. 2b, which shows the same solder bond after 155 h at 130 °C thermal aging, the microstructure of the joint is subject to ripening processes. The solder matrix coarsens to grain sizes of 10 μm to 30 μm. Additionally, the formation of a Cu_3Sn phase in between the Cu_6Sn_5 and the Cu core is observed as well as a further growth of the already existing IMCs. After this aging step, the Cu_6Sn_5 phase measures up to a thickness of 1 μm to 1.5 μm, whereas the Ag_3Sn phase reaches 4 μm to 6 μm. It is observed that Sn penetrates the busbar locally and approaches the wafer surface.

The cross section of the Sn60Pb40 solder joint aged for 750 h is shown in Fig. 2c. The ongoing coarsening process of the solder matrix leads to a separation of Sn and Pb phases into very few individual, large grains. Occasionally, fine cracks within phases are observed, which can lower the fatigue resistance of the solder joint and may be responsible for a gradual series resistance increase of the interconnection. At the contacted areas, the IMC growth eventually results in the entire consumption of the underlying metallization by the Ag_3Sn phase. Possible consequences are discussed in section 4. The Cu_6Sn_5 phase reaches a thickness of 1.5 μm to 2.5 μm, the Cu_3Sn phase is 1 μm to 2 μm.
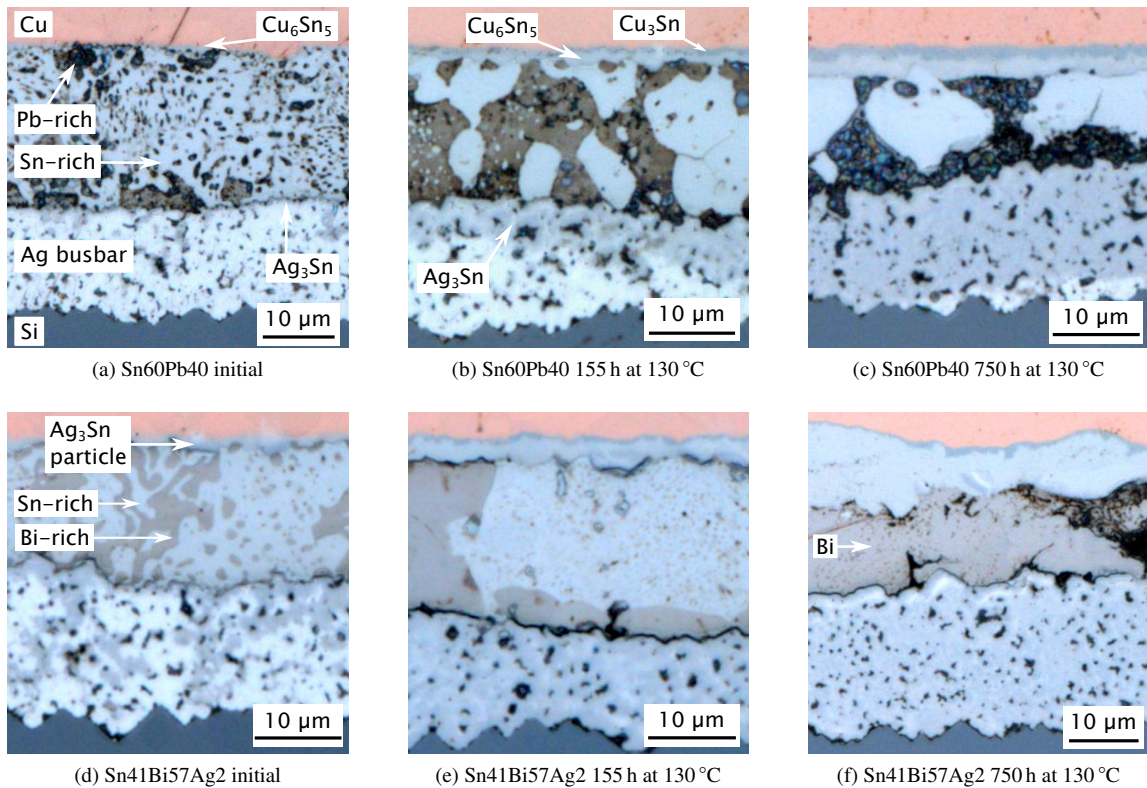
Fig. 2. Microstructural changes during thermal aging of solar cell interconnections.

The initial Sn41Bi57Ag2 bond (Fig. 2d) is characterized by a similarly fine initial distribution of Bi and Sn crystals in the solder matrix. The Ag-addition in the solder is to refine the microstructure and to improve the mechanical strength of the solder [22]. The Ag-content is primarily bonded as Ag_3Sn compounds attached to the interface to the copper core of the ribbon. These Ag_3Sn particles have a diameter of 1 μm to 2 μm. The initial Cu_6Sn_5 intermetallic phase is slightly thicker as compared to the Sn60Pb40 solder joint with 0.6 μm. Furthermore, the initial Ag_3Sn layer is between 0.8 μm to 0.9 μm, which marginally exceeds the initial Ag_3Sn thickness of the Sn60Pb40 solder bond. However, already in the initial condition Sn penetrates deeply into the busbar.

Following thermal aging for 155 h at 130 °C, which is a comparably high homologous temperature for Sn41Bi57Ag2, the solder matrix rapidly coarsens to large Bi-rich and Sn-rich phases (Fig. 2e). However, within the Sn phase a uniform distribution of fine Bi grains with a diameter of below 1 μm is observed. The intermetallic layer growth at the interfaces to the substrates proceeds faster as compared to the Sn60Pb40 solder. Already after 155 h aging time the whole contacted busbar is transformed into Ag_3Sn. The Cu_6Sn_5 phase is at 2 μm to 3 μm, and the Cu_3Sn phase reaches ≈1 μm.

When the Sn41Bi57Ag2 solder bond is thermally aged for 750 h at 130 °C, the solder matrix is entirely depleted of Sn and the Bi phase remains isolated between the ribbon and busbar (see Fig. 2f). Moreover, cracks and cavities are formed in the Bi-layer, which is due to the brittle nature of the metal. These cracks and cavities will very likely reduce the ability of the joint to resist thermomechanical stress and are expected to lead to a significant module degradation. Furthermore, it is observed that the Cu_6Sn_5 phase grows excessively to a thickness of 8 μm to 12 μm.

The thickness of the IMCs is measured after each aging step. The results of the measurements are shown in Fig. 3 as symbols. This data is converted to Arrhenius plots to extract the activation energy of the growth process. As an example, the Arrhenius plot for the growth of Ag_3Sn using a Sn41Bi57Ag2 solder is shown in Fig. 4.

The kinetic parameters of the IMC growth are given in Table 2, and may be used with equation 3 to estimate the
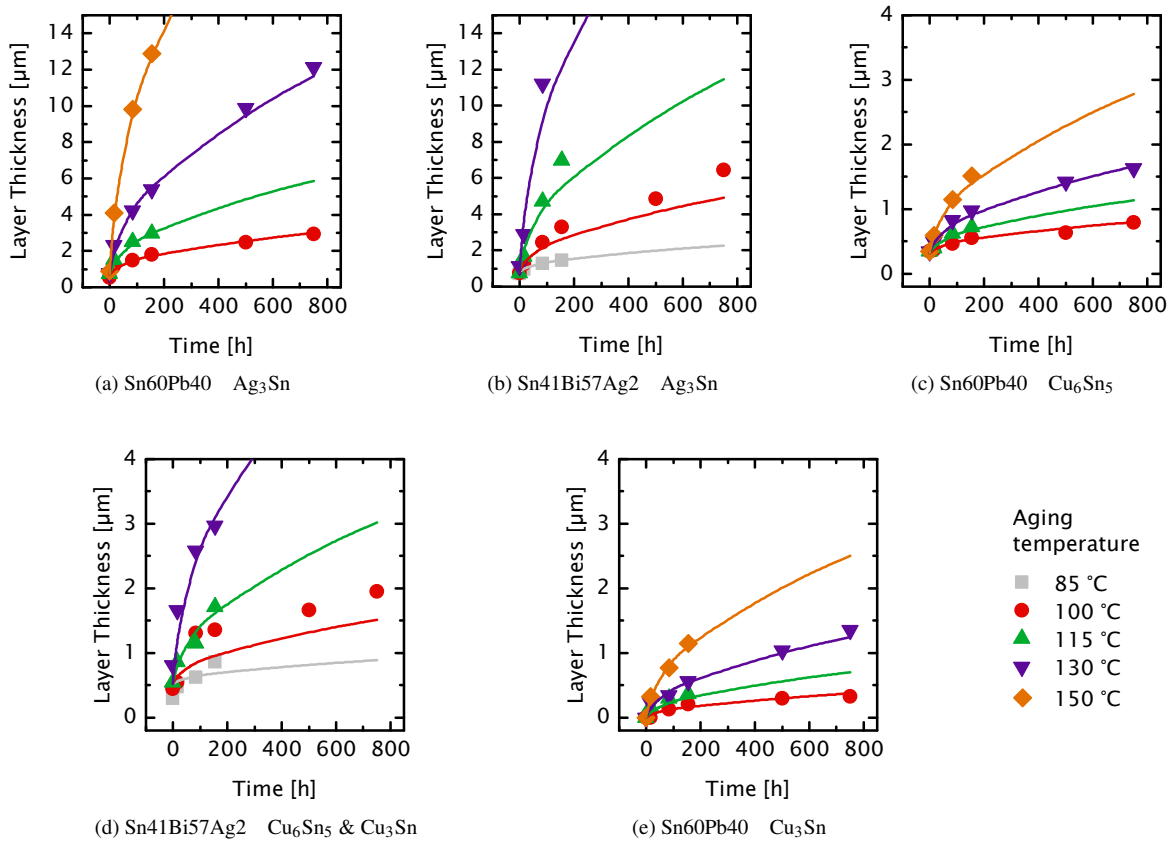
Fig. 3. Experimentally determined IMC growth (symbols) and simulated IMC growth (lines). The Cu_6Sn_5 and Cu_3Sn IMCs are consolidated in the analysis of Sn41Bi57Ag2 solder joints because in samples with low solder depot Cu_3Sn grows in expense of Cu_6Sn_5, that can occasionally lead to a thickness reduction of Cu_6Sn_5 as reported in reference [5]. This circumstance would lead to larger deviations in the determination of the kinetic parameters. The combination of both phases allows a simplified analysis of the effective IMC growth. Please note that samples with Sn43Bi57Ag2 are thermally aged from 85 °C to 130 °C due to the limitation of the low melting point whereas Sn60Pb40 is aged from 100 °C to 150 °C.
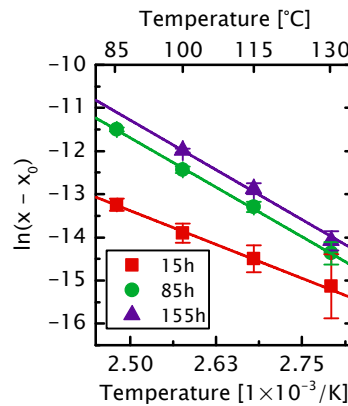

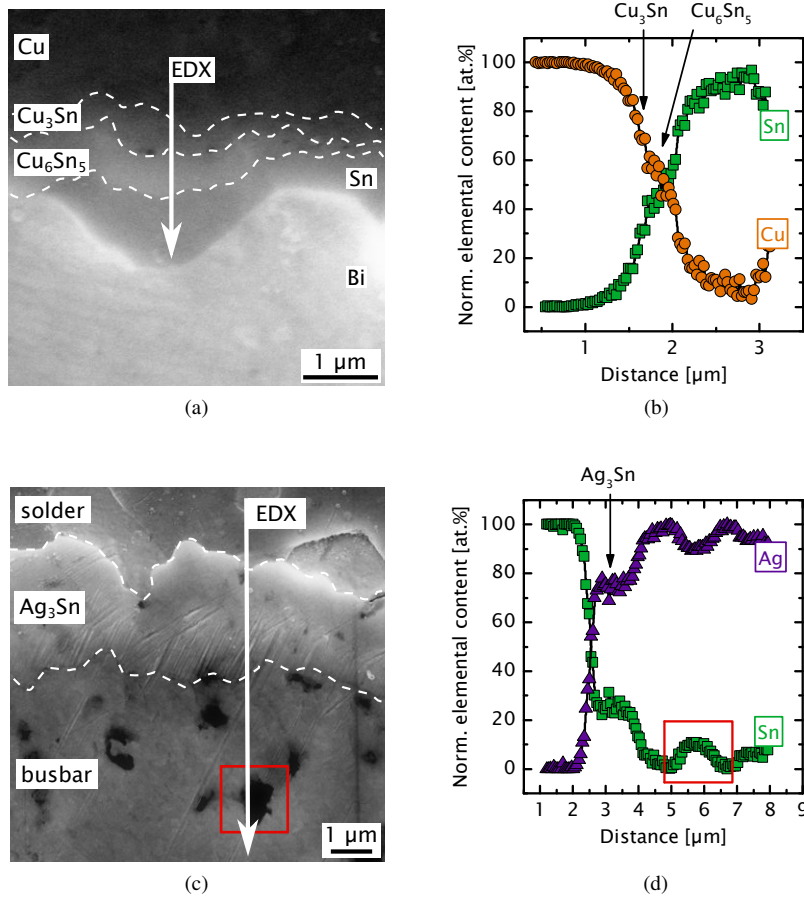Fig. 4. Arrhenius plot of the growth of Ag_3Sn using Sn41Bi57Ag2 solder.

Fig. 5. (a) SEM image of the interface from copper core to Sn41Bi57Ag2 with Cu_6Sn_5 and Cu_3Sn intermetallic layers after thermal aging at 100 °C for 155 h (b) EDX line scan across this Cu-solder-interface. (c) SEM image of the interface from Sn41Bi57Ag2 to busbar after thermal aging at 100 °C for 85 h. (d) EDX line scan across the same solder-busbar-interface. The red rectangle highlights a cavity in the busbar with accumulated Sn.

phase growth for arbitrary isothermal conditions[2]. The lines in Fig. 3 represent simulated phase growth with the methods described in this paper. The mean absolute error (MAE) is used as a measure to describe the predictability of the simulation [23]. It is between 0.1 µm to 1.8 µm indicating a good fit between experiment and calculation.

3.2. EDX analysis of the interfaces

A SEM detail of the Cu-solder-interface using Sn41Bi57Ag2 thermally aged for 155 h at 100 °C is shown in Fig. 5a. Supplementary, Fig. 5b depicts the quantitative EDX line scan across this interface. At the region of the Cu_6Sn_5-IMC an elemental content of 45 at.% to 60 at.% Cu and, proportionately 40 at.% to 55 at.% Sn is found, which is close to the predicted ratio of 55 at.% Cu and 45 at.% Sn. The Cu_3Sn phase is more difficult to resolve as no particular plateau is observed in the available data due to limitations of the measurement.

Correspondingly, a SEM detail of the solder-busbar-interface is shown in Fig. 5c. A cavity in the busbar is highlighted with a red rectangle. Additionally, in Fig. 5d the EDX line scan is shown across this interface. As expected, the region of the uniform Ag_3Sn layer directly at the interface to the solder has the elemental content of 70 at.% to 75 at.% Ag and 25 at.% to 30 at.% Sn, which is predicted by the Ag-Sn phase diagram [18]. It is important to note that,

---

[2]The activation energy Q may alternatively be expressed in electron volts (eV) if the relation between gas constant R, Boltzmann constant k_B and Avogadro constant N_A is considered, which has the form $R = k_B \cdot N_A$. Hence, if the activation energy in J mol^{-1} is divided by N_A in mol^{-1} the resulting energy can be expressed in eV.

Table 2. Kinetic parameters of the intermetallic phase growth. The weighted average of the activation energy of the three time series (15 h, 85 h and 155 h) as well as the weighted average of the pre-exponential factor as determined by non-linear fitting is given. The error values attached to the activation energy show the (average) standard error of the linear fits in the Arrhenius plots. The error values attached to the pre-exponential factor is the standard error from the non-linear fit.

Solder coating	IMC	Q [kJ mol^{-1}]	D_0 [m^2 s^{-1}]	x_0 [μm]
Sn60Pb40	Ag$_3$Sn	129.7 ± 3.9	1.44 ± 0.04	0.70
Sn60Pb40	Cu$_6$Sn$_5$	85.7 ± 4.6	$4.25 \times 10^{-8} \pm 0.15 \times 10^{-8}$	0.32
Sn60Pb40	Cu$_3$Sn	99.4 ± 6.2	$2.20 \times 10^{-6} \pm 0.16 \times 10^{-6}$	0.00
Sn41Bi57Ag2	Ag$_3$Sn	153.2 ± 7.3	$8.60 \times 10^{3} \pm 1.07 \times 10^{3}$	0.83
Sn41Bi57Ag2	Cu$_6$Sn$_5$ + Cu$_3$Sn	147.7 ± 31.5	88.5 ± 15.6	0.52

besides the continuous Ag$_3$Sn-layer, non-uniform and locally distributed Sn agglomerations are found, in particular, around cavities such as highlighted in Fig. 5c. These are interpreted as ζ-(Ag), but also (Ag) with upto 11.5 at.% Sn in solid solution is conceivable [18].

3.3. Modeling of intermetallic phase growth

The kinetic parameters allow to prognosticate the intermetallic layer thickness in accelerated aging tests or outdoor conditions using the respective temperature profiles as an input. It is of interest to estimate the phase growth during the PV module reliability tests damp heat, which is done at a constant 85 °C, and thermal cycling of −40 °C to 85 °C at a cycle time of ≈2.8 h [13]. Note that any possible influence other than temperature is not included in the estimation.

The phase growth over the number of cycles during thermal cycling is shown in Fig. 6a. It is estimated that a rather limited phase growth as compared to isothermal aging at elevated temperatures occurs, which is due to the limited amount of time that the solder bond is at elevated temperatures. In the worst case, the Ag$_3$Sn layer thickness is 1.5 μm for Sn41Bi57Ag2. Differently from that, the IMC growth reaches 3.7 μm in case of Ag$_3$Sn with Sn41Bi57Ag2 and 2.6 μm in case of Ag$_3$Sn with Sn60Pb40 respectively after 3000 h at 85 °C (see Fig. 6b).

Furthermore, it is useful to make a prognosis of the IMC growth at realistic outdoor conditions. For this purpose, temperature data of a PV module installed in Freiburg, Germany over the course of one year (June, 01 2012 – May, 15 2013) is considered (Fig. 7a). This one year curve is iterated 25 times in order to estimate the temperature progression for 25 years.

The simulation for the course of the first year is shown in Fig. 7b. It is apparent that the Ag$_3$Sn-layer grows 0.1 μm during summer and, as expected, stops to grow during winter. In spring of the following year phase growth proceeds due to the increasing temperature. This form of sequential increase and stagnation of layer thickness is evident over the
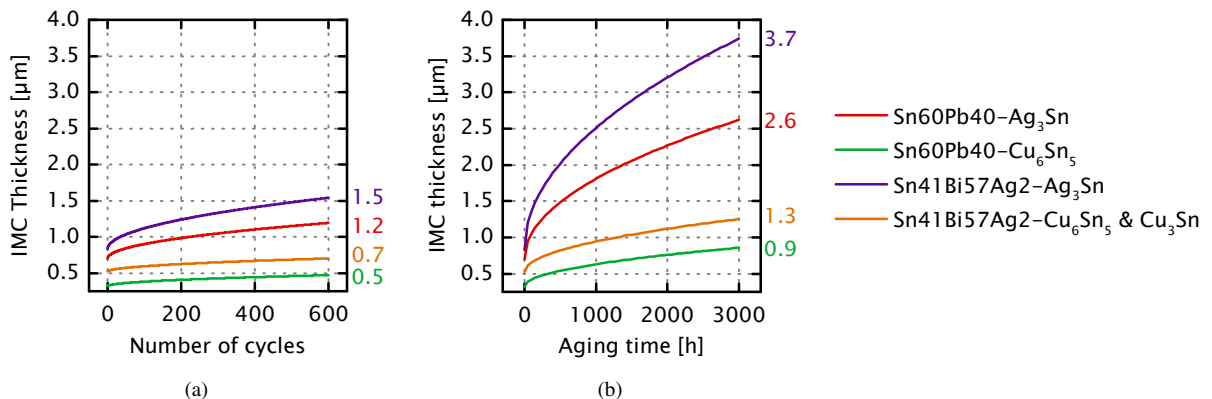

Fig. 6. (a) Predicted IMC thickness during thermal cycling between −40 °C to 85 °C. (b) Predicted IMC thickness during constant 85 °C.
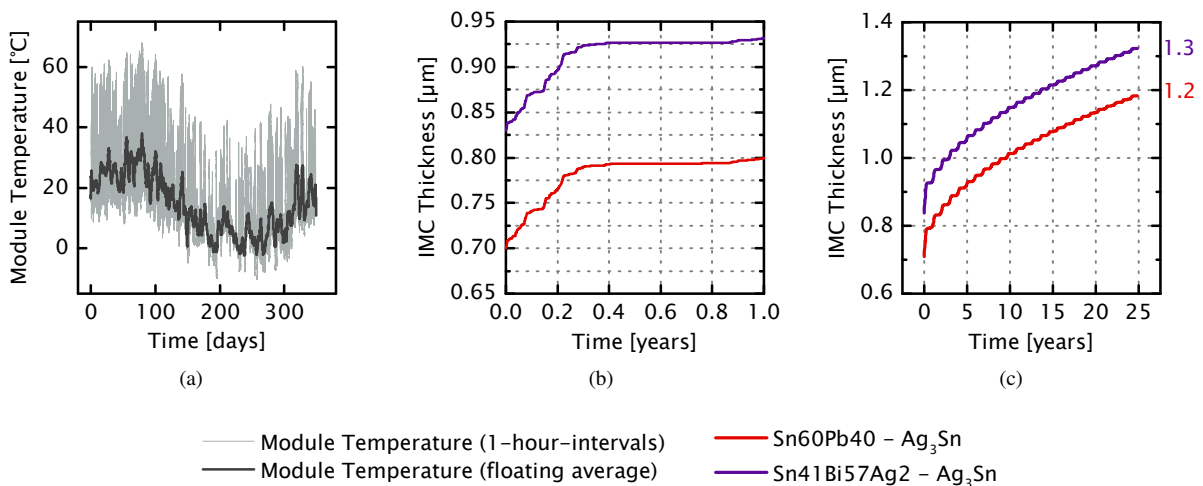
Fig. 7. (a) Temperature development in a crystalline Si module over the course of one year in Freiburg, Germany beginning from June 01, 2012 to May 15, 2013. (b) Growth of the Ag$_3$Sn phase within Sn60Pb40 and Sn41Bi57Ag2 during the first year of outdoor exposure. (c) IMC growth during 25 years in Freiburg.

course of 25 years as a step-wise growth curve shown in Fig. 7c. It is noteworthy that the predicted IMC thickness is rather thin with 1.3 µm for Ag$_3$Sn in Sn41Bi57Ag2 solder joints and 1.2 µm for Ag$_3$Sn in Sn60Pb40 solder bonds, which is well achieved within 1000 h at 85 °C. The reason for the limited predicted phase growth during outdoor exposure is the low module temperature that rarely exceeds 60 °C. IMCs will grow more in desert regions with a higher module temperature. Moreover, no significant differences between the IMC growth kinetics of Sn60Pb40 and Sn41Bi57Ag2 is prognosticated under these conditions. The final differences in the phase thickness are only due to the initial differences in IMC thickness.

4. Discussion

During thermal aging of solder bonds extended microstructural changes are observed in the solder matrix and at the interfaces to the busbar and the copper ribbon. Grain coarsening generally leads to a reduction in bond strength of solder joints and is a major reliability problem in electronics. Especially when intermetallics are still thin, embrittlement due to grain coarsening can be the dominant failure mode [24, 25, 26]. Investigations of field aged PV modules reveal that fatigue cracking within coarsened solder joints is commonly observed after prolonged outdoor exposure [27, 28, 29, 30].

In section 3.1 it is presented that grain coarsening is accelerated in Sn41Bi57Ag2 solder bonds as compared to Sn60Pb40. In particular if the solder layer is thin, the solder matrix can be entirely depleted of Sn after a short to medium thermal aging duration with only a layer of Bi remaining. Since Bi is a brittle material, it is very likely that fatigue resistance is reduced for these solder bonds as has already been shown with the comparable solder Sn42Bi58 [31]. On the basis of our observations, we expect higher risks for PV module reliability when Sn41Bi57Ag2 is used. Further work, in terms of reliability testing, outdoor performance monitoring of Sn41Bi57Ag2 joints is necessary before it can replace Sn60Pb40.

Additionally, the phenomenon of Sn penetration into the busbar during the soldering process as well as during thermal aging, regardless of using Sn60Pb40 or Sn41Bi57Ag2, are deemed as risks for the reliability of the interconnection. Sn agglomeration and IMC formation in the busbar seem to be localized around cavities and lead-glass particles. We assume this to be caused by a higher diffusivity of Sn atoms from the solder along the cavities, lead-glass particles and defects in the busbar as compared to the diffusivity of Sn in solid Ag.

Previous research already indicates the reduction of mechanical strength of solar cell interconnections due to Sn penetrating into the busbar [9]. From our experience, the failed interface during a 90° or 180° peel test after thermal

aging is predominately the busbar metallization to the wafer while the glass frit remains on the wafer surface. The effect of adhesion loss of the metallization is known in hybrid thick-film technology for several decades [32, 33]. Crossland and Hailes discuss that the reduction in mechanical strength between metallization and substrate is due to the swelling of the metallization once Sn penetrates into it and forms intermetallic compounds [33]. Loasby et. al. concretize that diffusion swelling instead of intermetallic phase formation is believed to be the primary cause of adhesion failure of the glass frit as part of the metallization [34]. Furthermore, Taylor et. al. explain that swelling cannot be the sole reason for adhesion loss since two- to threefold volume increase in the metallization can be observed without the loss of adhesion [35]. Instead, a reduction reaction of bismuth oxide, which is part of the binder component of the paste used in their study, into bismuth metal by diffused Sn atoms is assumed to destroy the oxide bonding of the metallization. This reference only offers a brief explanation of the adhesion failure since in solar cell screen-printing pastes lead oxide is typically involved and not bismuth oxide. However, a comparable degradation mechanism cannot be ruled out.

Ensuing from the discussion, the phenomenon of Sn penetration has a detrimental effect on metallization adhesion properties. It is still largely unclear to what extent this loss of adhesion influences the performance of PV modules during accelerated aging tests and outdoor exposure. Further research in this field should be directed to understanding the impact of intermetallic compounds within solder bonds on the reliability of PV modules and specifically to investigating the effect of adhesion loss of the metallization due to Sn penetration.

Approaches to prevent extensive intermetallic phase growth and/or the loss of adhesion are already presented in literature. The use of alternative solder materials on the side of the interconnection technology is claimed to reduce phase growth and maintain peel strength during thermal aging [9, 11]. Additionally, developments in paste chemistry on the side of the metallization technology are an option [36].

It must be clarified that our observations of microstructural changes are solely based on studies under isothermal aging conditions. Since the growth process of intermetallic compound layers mainly depends on temperature, this experimental approach is usually sufficient. Other environmental factors such as humidity are not expected to impact our quantitative analysis of IMC growth.

However, microstructural changes under isothermal conditions should be clearly distinguished between changes in solder joints which occur during module testing according to IEC tests or during outdoor exposure. The IEC test sequence includes 200 thermal cycles from $-40\,°C$ to $85\,°C$ and damp heat exposure for $1000\,h$ at $85\,°C$ combined with $85\,\%$ RH [13]. Under these test conditions, it is expected that the changes in the solder microstructure are dominated by crack growth between grains in the solder matrix and at the interface from solder to ribbon and to cell metallization. This is caused by the CTE-mismatch and following build-up of thermomechanical stress between Si-wafer and Cu-ribbon. The solder layer only possesses a limited capability to compensate for the thermomechanical stress. Moreover, the ingress of water vapor into the PV module leads to the release of acetic acid from the ethylen-vinyl acetate encapsulant. This, furthermore, determines a corrosion and ablation of the cell metallization. Since these topics are beyond the scope of this paper, the reader is referred to other published research dealing more specifically with those degradation modes [29, 30, 37, 38, 39].

The simulation of the IMC growth is based on a purely thermally-driven diffusion process, and we find good agreement between calculation and experimental data for short term thermal aging up to $750\,h$ at elevated temperatures above $85\,°C$ with a maximum MAE of $1.8\,\mu m$ (see Figure 3). However, our simulation of IMC growth under outdoor conditions and under extended IEC tests still lacks a cross-check with experimental data and should be considered as a prognosis based on a thermally-driven process, that strictly obeys the Arrhenius relationship with one single activation energy.

5. Conclusion

The formation of thin and uniform intermetallic layers at the interface to the Cu ribbon and the Ag busbar is part of the pre-tinning and soldering process, respectively and an indication for a proper metallurgical bond. Initially, a $0.3\,\mu m$ to $0.6\,\mu m$ Cu_6Sn_5 intermetallic layer of scallop-shape morphology is found at the interface to the Cu ribbon when Sn60Pb40 or Sn41Bi57Ag2 solder alloys are used. At the interface to the Ag busbar a $0.7\,\mu m$ to $0.9\,\mu m$ Ag_3Sn layer is observed, and local Sn penetration especially at cavities and around lead-glass particles is found.

The microstructure of solder joints changes drastically during thermal aging. Grain coarsening, further Sn pene-tration into the busbar and intermetallic phase growth at the soldered areas of the busbar and ribbon take place, that

have an impact on the reliability of the solder joint. The operation of Sn41Bi57Ag2 solder at a higher homologous temperature compared to Sn60Pb40 leads to an accelerated phase growth and grain coarsening. It is observed that the solder matrix is entirely depleted of Sn and a sole Bi layer is remaining after mid to long term thermal aging. This likely reduces the fatigue resistance of Sn41Bi57Ag2 solder joints due to the brittle nature of bismuth.

The intermetallic phase growth is modeled using the mean square diffusion distance and the Arrhenius relationship, and enables the development of customized accelerated aging tests. It is predicted that a constant temperature of 85 °C for 3000 h, as present in PV module damp heat tests, leads to an Ag_3Sn phase thickness of 3.7 µm with Sn41Bi57Ag2 solder and 2.6 µm with Sn60Pb40. The thermal budget of 600 thermal cycles is calculated to result in only 1.5 µm Ag_3Sn for Sn41Bi57Ag2 and 1.2 µm Ag_3Sn for Sn60Pb40, respectively. Our model for the thermally-driven intermetallic phase growth over 25 years in the outdoor location Freiburg, Germany predicts 1.3 µm Ag_3Sn for Sn41Bi57Ag2 and 1.2 µm Ag_3Sn for Sn60Pb40.

References

[1] M. A. Green, Commercial progress and challenges for photovoltaics, Nature Energy 1 (1) (2016) 1–4. doi:10.1038/NENERGY.2015.15.

[2] T. Laurila, V. Vuorinen, J. K. Kivilahti, Interfacial reactions between lead-free solders and common base materials, Materials Science and Engineering: R: Reports 49 (1-2) (2005) 1–60. doi:10.1016/j.mser.2005.03.001.

[3] J. O. G. Parent, D. D. L. Chung, I. M. Bernstein, Effects of intermetallic formation at the interface between copper and lead-tin solder, Journal of Materials Science 23 (7) (1988) 2564–2572. doi:10.1007/BF01111916.

[4] D. R. Frear, P. T. Vianco, Intermetallic growth and mechanical behavior of low and high melting temperature solder alloys, Metallurgical and Materials Transactions A 25 (7) (1994) 1509–1523. doi:10.1007/BF02665483.

[5] A. C. K. So, Y. C. Chan, J. Lai, Aging studies of Cu-Sn intermetallic compounds in annealed surface mount solder joints, IEEE Transactions on Components, Packaging, and Manufacturing Technology: Part B 20 (2) (1997) 161–166. doi:10.1109/ECTC.1996.550884.

[6] P. L. Tu, Y. C. Chan, J. Lai, Effect of intermetallic compounds on the thermal fatigue of surface mount solder joints, IEEE Transactions on Components, Packaging, and Manufacturing Technology: Part B 20 (1) (1997) 87–93. doi:10.1109/96.554534.

[7] K. Zeng, K. N. Tu, Six cases of reliability study of Pb-free solder joints in electronic packaging technology, Materials Science and Engineering: R: Reports 38 (2) (2002) 55–105. doi:10.1016/S0927-796X(02)00007-4.

[8] A. Faes, M. Despeisse, J. Levrat, J. Champliaud, N. Badel, M. Kiaee, T. Söderström, Y. Yao, R. Grischke, M. Gragert, J. Ufheil, P. Papet, B. Strahm, G. Cattaneo, J. Cattin, Y. Baumgartner, A. Hessler-Wyser, C. Ballif, Smartwire solar cell interconnection technology, in: Proceedings of the 29th European Photovoltaic Specialist Conference and Exhibition, 2014, pp. 2555–2561.

[9] P. Schmitt, P. Kaiser, C. Savio, M. Tranitz, U. Eitner, Intermetallic phase growth and reliability of Sn-Ag-soldered solar cell joints, Energy Procedia 27 (2012) 664–669. doi:10.1016/j.egypro.2012.07.126.

[10] V. Jung, M. Köntges, Al/NiV/Ag metal stacks as rear-side metallization for crystalline silicon solar cells, Progress in Photovoltaics: Research and Applications 21 (2012) 876–883. doi:10.1002/pip.2169.

[11] T. L. Yang, K. Y. Huang, S. Yang, H. H. Hsieh, C. R. Kao, Growth kinetics of Ag3Sn in silicon solar cells with a sintered Ag metallization layer, Solar Energy Materials and Solar Cells 123 (2014) 139–143. doi:10.1016/j.solmat.2014.01.018.

[12] D. Eberlein, P. Schmitt, P. Voos, Metallographic sample preparation of soldered solar cells, Practical Metallography 48 (5) (2011) 239–260.

[13] IEC 61215: 2005-04 Crystalline silicon terrestrial photovoltaic (PV) modules - Design qualification and type approval (2005).

[14] U. Goesele, K. N. Tu, Growth kinetics of planar binary diffusion couples: "Thin-film case" versus "bulk cases", Journal of Applied Physics 53 (4) (1982) 3252. doi:10.1063/1.331028.

[15] R. J. Borg, G. J. Dienes, An Introduction to Solid State Diffusion, Academic Press, San Diego, 1988.

[16] P. G. Harris, K. S. Chaggar, M. A. Whitmore, The effect of ageing on the microstructure of 60:40 tin–lead solders, Soldering & Surface Mount Technology 3 (1) (1991) 20–33. doi:10.1108/eb037741.

[17] N. Saunders, A. P. Miodownik, The Cu-Sn (copper-tin) system, Bulletin of Alloy Phase Diagrams 11 (3) (1990) 278–287. doi:10.1007/BF03029299.

[18] I. Karakaya, W. T. Thompson, The Ag-Sn (silver-tin) system, Bulletin of Alloy Phase Diagrams 8 (4) (1987) 340–347. doi:10.1007/BF02869270.

[19] H. K. Kim, H. K. Liou, K. N. Tu, Three-dimensional morphology of a very rough interface formed in the soldering reaction between eutectic SnPb and Cu, Applied Physics Letters 66 (18) (1995) 2337. doi:10.1063/1.113975.

[20] G. Zeng, S. Xue, L. Zhang, L. Gao, W. Dai, J. Luo, A review on the interfacial intermetallic compounds between Sn–Ag–Cu based solders and substrates, Journal of Materials Science: Materials in Electronics 21 (5) (2010) 421–440. doi:10.1007/s10854-010-0086-y.

[21] P. T. Vianco, R. D. Wright, P. F. Hlava, J. J. Martin, Dissolution and interface reactions between the 95.5Sn-3.9Ag-0.6Cu, 99.3Sn-0.7Cu, and 63Sn-37Pb solders on silver base metal, Metallurgical and Materials Transactions A 37 (5) (2006) 1551–1561. doi:10.1007/s11661-006-0099-6.

[22] M. McCormack, H. S. Chen, G. W. Kammlott, S. Jin, Significantly improved mechanical properties of Bi-Sn Solder alloys by Ag-doping, Journal of Electronic Materials 26 (8) (1997) 954–958. doi:10.1007/s11664-997-0281-7.

[23] D. G. Mayer, D. G. Butler, Statistical validation, Ecological Modelling 68 (1-2) (1993) 21–32. doi:10.1016/0304-3800(93)90105-2.

[24] D. Frear, D. Grivas, J. Morris, A microstructural study of the thermal fatigue failures of 60Sn-40Pb solder joints, Journal of Electronic Materials 17 (2) (1988) 171–180. doi:10.1007/BF02652148.

[25] H. Ma, J. C. Suhling, A review of mechanical properties of lead-free solders for electronic packaging, Journal of Materials Science 44 (5) (2009) 1141–1158. doi:10.1007/s10853-008-3125-9.

[26] Y. Tian, W. Liu, R. An, W. Zhang, L. Niu, C. Wang, Effect of intermetallic compounds on fracture behaviors of Sn3.0Ag0.5Cu lead-free solder joints during in situ tensile test, Journal of Materials Science: Materials in Electronics 23 (1) (2012) 136–147. doi:10.1007/s10854-011-0538-z.

[27] D. L. King, M. A. Quintana, J. A. Kratochvil, D. E. Ellibee, B. R. Hansen, Photovoltaic module performance and durability follow-ing long-term field exposure, Progress in Photovoltaics: Research and Applications 8 (2) (2000) 241–256. doi:10.1002/(SICI)1099-159X(200003/04)8:2<241::AID-PIP290>3.0.CO;2-D.

[28] M. A. Quintana, D. L. King, T. J. McMahon, C. R. Osterwald, Commonly observed degradation in field-aged photovoltaic modules, in: Conference Record of the Twenty-Ninth IEEE Photovoltaic Specialists Conference, 2002, pp. 1436–1439. doi:10.1109/PVSC.2002.1190879.

[29] U. Itoh, T. Nishimura, T. Fukami, K. Takamura, A. Kita, R. Miyabayashi, Solder joint failure modes in crystalline Si PV modules operated in Tsukuba, Japan for 10 years, in: IEEE (Ed.), Proceedings of the 40th IEEE Photovoltaic Specialist Conference, 2014, pp. 2021–2024. doi:10.1109/PVSC.2014.6925323.

[30] G. Cuddalorepatta, A. Dasgupta, S. Sealing, J. Moyer, T. Tolliver, J. Loman, Durability of Pb-free solder between copper interconnect and silicon in photovoltaic cells, Progress in Photovoltaics: Research and Applications 18 (3) (2010) 168–182. doi:10.1002/pip.944.

[31] Z. Mei, J. Morris, Characterization of eutectic Sn-Bi solder joints, Journal of Electronic Materials 21 (6) (1992) 599–607. doi:10.1007/BF02655427.

[32] A. A. Milgrim, Influence of metallic diffusion on the adhesion of screen printed silver films, Metallurgical and Materials Transactions B 1 (3) (1970) 695–700. doi:10.1007/BF02811597.

[33] W. A. Crossland, L. Hailes, Thick film conductor adhesion reliability, Solid State Technology (1971) 42–47.

[34] R. G. Loasby, N. Davey, H. Barlow, Enhanced property thick-film conductor pastes, Solid State Technology 15 (5) (1972) 46–50.

[35] B. Taylor, J. Felten, J. Larry, Progress in and technology of low-cost silver containing thick-film conductors, IEEE Transactions on Components, Hybrids, and Manufacturing Technology 3 (4) (1980) 504–517. doi:10.1109/TCHMT.1980.1135648.

[36] J. Moyer, W. Zhang, E. Kurtz, R. Tavares, D. Buzby, S. Kleinbach, The role of silver contact paste on reliable connectivity systems, in: Proceedings of the 25th Photovoltaic Solar Energy Conference and Exhibition / 5th World Conference on Photovoltaic Energy Conversion, 2010, pp. 2624–2630.

[37] C. Peike, S. Hoffmann, P. Hülsmann, B. Thaidigsmann, K. A. Weiß, M. Koehl, P. Bentz, Origin of damp-heat induced cell degradation, Solar Energy Materials and Solar Cells 116 (2013) 49–54. doi:10.1016/j.solmat.2013.03.022.

[38] A. Kraft, L. Labusch, T. Ensslen, I. Durr, J. Bartsch, M. Glatthaar, S. Glunz, H. Reinecke, Investigation of acetic acid corrosion impact on printed solar cell contacts, IEEE Journal of Photovoltaics 5 (3) (2015) 736–743. doi:10.1109/JPHOTOV.2015.2395146.

[39] J.-S. Jeong, N. Park, C. Han, Field failure mechanism study of solder interconnection for crystalline silicon photovoltaic module, Microelec-tronics Reliability 52 (9-10) (2012) 2326–2330. doi:10.1016/j.microrel.2012.06.027.